A Counterion-Catalyzed (S^0H^+)(X^-I^+) Pathway toward Heat- and Steam-Stable Mesostructured Silica Assembled from Amines in Acidic Conditions

Kristof Cassiers,*,† Pascal Van Der Voort,† Thierry Linssen,† Etienne F. Vansant,† Oleg Lebedev,‡ and Joseph Van Landuyt‡

Department of Chemistry, Laboratory of Adsorption and Catalysis, University of Antwerp (UIA), Universiteitsplein 1, B-2610 Wilrijk, Belgium, and Centre for Electron Microscopy and Materials Science, University of Antwerp (RUCA), Groenenborgerlaan 171, B-2020 Antwerpen, Belgium

Received: August 6, 2002; In Final Form: December 5, 2002

An alternative pathway to assemble mesoporous molecular sieve silicas is developed using nonionic alkylamines and *N*,*N*-dimethylalkylamines (S^0) as structure-directing agents in acidic conditions. The synthesized mesostructures possess wormhole-like frameworks with pore sizes and pore volumes in the range of 20−90 Å and 0.5−1.3 cm^3/g, respectively. The formation of the mesophase is controlled by a counterion-mediated mechanism of the type (S^0H^+)(X^-I^+), where S^0H^+ are protonated water molecules that are hydrogen bonded to the lone electron pairs on the amine surfactant headgroups (S^0H^+), X^- is the counteranion originating from the acid, and I^+ are the positively charged (protonated) silicate species. We found that the stronger the ion X^- is bonded to S^0H^+, the more it catalyzes the silica condensation into (S^0H^+)(X^-I^+). Br^- is shown to be a strong binding anion and therefore a fast silica polymerization promoter compared to Cl^- resulting in the formation of a higher quality mesophase for the Br^- syntheses. We also showed that the polymerization rate of the silica, dictated by the counterion, controls the morphology of the mesostructures from nonuniform agglomerated blocks in the case of Br^- syntheses to spherical particles for the Cl^- syntheses. Next to many benefits such as low temperature, short synthesis time, and the use of inexpensive, nontoxic, and easily extractable amine templates, the developed materials have a remarkable higher thermal and hydrothermal stability compared to hexagonal mesoporous silica, which is also prepared with nonionic amines but formed through the S^0I^0 mechanism.

Introduction

Enormous efforts are being devoted to the preparation of mesoporous molecular sieves by using a supramolecular templating approach. The development of templated mesoporous inorganic frameworks such as M41S (MCM-41 and MCM-48),[1] FSM-16,[2] KIT-1,[3] PCH,[4] HMS,[5,6] SBA-*n* (n = 1−16),[7−9] MSU-*X* (X = 1−4),[10] MSU-*n* (n = H,[11] V,[12] F,[11] G,[13]), MCF,[14] and PHTS[15] has made available a number of materials having pore diameters in the range of 2−40 nm with a variety of particle sizes, morphologies, and crystallographic symmetries. These materials have been reported to have potential applications in different areas such as homogeneous and heterogeneous catalysis[16] and gas and liquid chromatographic separation,[17,18] and recently, the templating technology broke new ground in the synthesis of metal nanowires,[19−21] ordered mesoporous carbons,[22,23] carbon nanotubes as probes for atomic force microscopy,[24] silica fibers,[25] and optoelectronic dye-doped mesostructures for potential laser applications.[26]

In general, two types of surfactants are used for the synthesis of mesoporous silica: ionic templates such as alkyltrimethylammonium bromide[1,2,7] and nonionic templates such as alkylamines[5] and poly(ethylene oxide)-type copolymers.[8,10,14,15]

The formation of M41S materials is based on charge-matching interactions between cationic surfactants (S^+) with inorganic reagents (I^-) in alkaline medium exhibiting bidimensional hexagonal *p*6*m* (MCM-41) or bicontinuous cubic *Ia*3*d* (MCM-48) pore architectures. Similarly, a layered silicate can be intercalated with cationic surfactants and can be transformed to FSM-16,[2] which has also a hexagonal *p*6*m* ordering. Additionally, SBA-1 (cubic discontinuous *Pm*3*n*), SBA-2 (hexagonal tridimensional *P*6/*mmc*), and SBA-3 (hexagonal bidimensional *p*6*m*) are formed in strongly acidic conditions through an anion-mediated mechanism between cationic surfactants and positively charged silicate species ($S^+X^-I^+$).[7]

Complementary to the ionic surfactants, two types of nonionic surfactants can be used for the synthesis of different mesocomposites. Pinnavaia and co-workers[5,6] reported the synthesis of hexagonal mesoporous silica (HMS) materials, which are formed by H-bonding interactions between neutral alkylamine templates (S^0) and electrically neutral silica precursors (I^0). Second, in the range of poly(ethylene oxide)-type (PEO) nonionic surfactants, two families of mesostructures can be identified: the MSU-*X* materials[10] prepared in near-neutral pH and the SBA-15 and -16 materials,[8,9] synthesized at a pH lower than 1. Similar to the mechanism of HMS, MSU-*X* compounds have been prepared through a supramolecular N^0I^0 pathway. Depending on N^0, a whole family of MSU-*X* materials (X = 1−4) can be prepared, where *X* refers to either alkyl PEO, alkyl aryl PEO, poly(propylene oxide) PEO block copolymers, or ethoxylated derivatives of sorbitan fatty esters, respectively.[10] SBA-15 and SBA-16, with two-dimensional hexagonal *p*6*m* and cubic Im3*m* ordering, respectively, are assembled under strongly acidic

† University of Antwerp (UIA).
‡ University of Antwerp (RUCA).
* Corresponding author. E-mail: kristof.cassiers@ua.ac.be.

10.1021/jp026696v CCC: $25.00
Published on Web 03/22/2003

aqueous media to allow for counterion-mediated interactions of the type (N^0H^+)(X^-I^+), where X^- is the counteranion, I^+ are the positively charged (protonated) silicate species, and N^0H^+ are hydronium ions associated with the alkylene oxygen atoms of the neutral block copolymers.

Similar to the electrostatically assembled mesocomposites such as M41S materials, SBA-15 and -16 materials have well-ordered channel and cage structures. In contrast, assembly pathways that exclusively utilize H-bonding or van der Waals interactions, such as S^0I^0 (HMS) and N^0I^0 (MSU), afford structures with wormholelike channel motifs and poorly defined crystallographic frameworks. However, despite the nonuniformity of the channel packing, the diameters of the channels of HMS- and MSU-type mesotructures are uniform. These wormholelike neutral assembled materials offer several attractive features.[5,10] First, the synthesis of these materials can be carried out at relative low reaction temperatures (25−70 °C) at atmospheric pressure that does not request specific autoclaves. Furthermore, the neutral templates are relative low cost and less toxic compared to ionic templates and can be easily recovered by a simple solvent extraction procedure using ethanol as extraction solvent[5] or by using acidified water[27] without sacrificing the physical properties such as pore size and surface area. Besides, mesoporous silicas with wormholelike framework structure have in general an enhanced reactivity in heterogeneous catalysis compared to their highly ordered hexagonal analogues.[28,29] This higher activity has been attributed to a three-dimensionally branched pore network for MSU and HMS supplemented by a complementary interparticullar (textural) porosity for HMS, allowing a facilitated access to reactive sites into the framework.

In the present work, we describe an alternative synthesis route to heat- and steam-stable mesoporous silica with wormholelike pore architecture in which many of the benefits listed above are combined such as low temperature and short-time synthesis and the use of inexpensive, nontoxic, and easily extractable amine templates. A new pathway, denoted (S^0H^+)(X^-I^+), is proposed, where the nonionic alkylamines, also used for the S^0I^0 pathway to HMS, and *N*,*N*-dimethylalkylamines (S^0) are assembled in strongly acidic conditions. Parallel to the synthesis route of SBA-15 and -16, where hydronium ions are associated with the alkylene oxygen atoms of the representative template, hydronium ions associated with the nitrogen atom of the amine surfactants are interacting with protonated silicate species, bringing the process under counterion-mediated electrostatic control. The influence on the structure quality of the reaction temperature, nature of the template, counterion, formation mechanism, and morphology will be discussed and the thermal and hydrothermal stability of these materials will be compared to the stability of S^0I^0-assembled HMS.

Experimental Section

(a) Sample Preparation. *Mesoporous Silica by (S^0H^+)(X^-I^+) Assembly.* For the syntheses of these materials, two kinds of amine templates were used, in particular primary alkylamines (dodecylamine and hexadecylamine) and *N*,*N*-dimethylalkylamines (*N*,*N*-dimethyldodecylamine and *N*,*N*-dimethylhexadecylamine). Materials synthesized with primary amines are further named as C_x-MS-Y and mesostructures prepared with *N*,*N*-dimethylamines are further denoted as NNC_x-MS-Y, where *x* stands for the alkyl chain length, MS for mesoporous silica, and Y for the counterion from the used acid (Cl or Br). In a typical synthesis, 0.012 mol of template was added to 100 mL of 2 M acid solution (HCl or HBr) and the solution was brought to a temperature of 25 or 70 °C and stirred for 15 min. Additionally, 0.036 mol of tetraethyl orthosilicate (TEOS) was added and the solution was stirred for 18 h at the same temperature in a closed system to avoid evaporation. The resulting product was filtered, washed thoroughly with distilled water, and dried at room temperature. The final product was then calcined from room temperature up to 550 °C with a heating rate of 2 °C/min and was kept at 550 °C for 8 h.

Mesoporous Silica by S^0I^0 Assembly (HMS). HMS was synthesized at room temperature according to the synthesis reported in literature[30] using dodecylamine (DDA) as structure directing agent and TEOS as silica source with molar ratios TEOS/DDA/ethanol/H_2O = 1/0.27/9.09/29.6. DDA was first dissolved in ethanol. To this mixture, the water was added followed by the addition of TEOS. After stirring for 18 h, the white solid was filtered, air-dried, calcined at 550 °C with a heating rate of 2 °C/min, and kept at 550 °C for 8 h.

(b) Instrumentation. X-ray diffractograms were recorded on a Philips PW1840 powder diffractometer, using Ni-filtered Cu Kα radiation.

Porosity and surface area studies were performed on a Quantachrome Autosorb-1-MP automated gas adsorption system. All samples were outgassed for 16 h at 200 °C prior to adsorption. Gas adsorption occurred using nitrogen as the adsorbate at liquid nitrogen temperature (77 K).

Scanning electron microscopy (SEM) images were recorded using a JEOL-JSM-6300 scanning electron microscope operating at an accelerating voltage of 20−30 kV. The samples were sputtered with a thin film of gold.

Transmission electron micrograph (TEM) images were recorded using a JEOL-4000-EX microscope operated at 400 kV to analyze the framework structure of the developed material.

(c) Stability Tests. *Thermal Stability.* To assess thermal stability, the samples were calcined in air starting from an end temperature of 550 °C. The end temperature was each time increased by 100 °C as long as no complete collapse of the concerned mesostructure had occurred. All the sample precursors were calcined with a heating rate of 2 °C/min and kept at the end temperature for 8 h.

Hydrothermal Stability. The hydrothermal stability study was conducted by exposing the samples to an N_2 stream containing 30 vol % water vapor at 400 °C for 48 and 120 h. The flow of the N_2 stream was kept at 100 mL/min with a pressure of 1 atm.

(d) Calculation Methods. Surface areas were calculated according to the BET equation[31] using adsorption data in a relative range from 0.05 to 0.3. Mesopore size distributions were calculated using the BJH method. Mesopore volumes (V_{mes}) were measured after the capillary condensation step. To calculate the mesopore size, it is generally agreed that the maximum of the BJH method underestimates the size of pores.[32,33] Therefore, the mesopore size was evaluated by means of the relative pressure−pore diameter relations developed by Neimark et al.[34,35] based on the nonlocal density functional theory. The mesopore size was calculated from the inflection point of the adsorption branch of the isotherm.

Results and Discussion

(a) General Features of Synthesized Materials. All of the materials synthesized in this work exhibit a single first-order d_{100} reflection in the X-ray diffraction pattern (Figure 1) corresponding to a pore center-to-pore center correlation length with a broad shoulder in the 2θ range 3−5. Furthermore, the formation of "meso" structures by this new pathway is supported

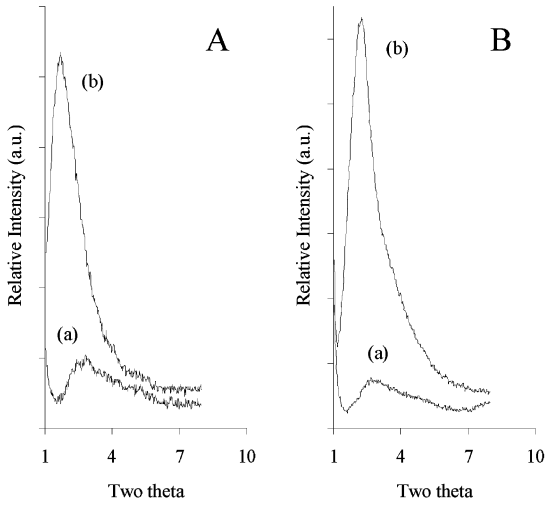

Figure 1. Powder X-ray diffraction patterns of C_{16}-MS-Br (A) and NNC_{16}-MS-Br (B) prepared at 25 (a) and 70 °C (b).

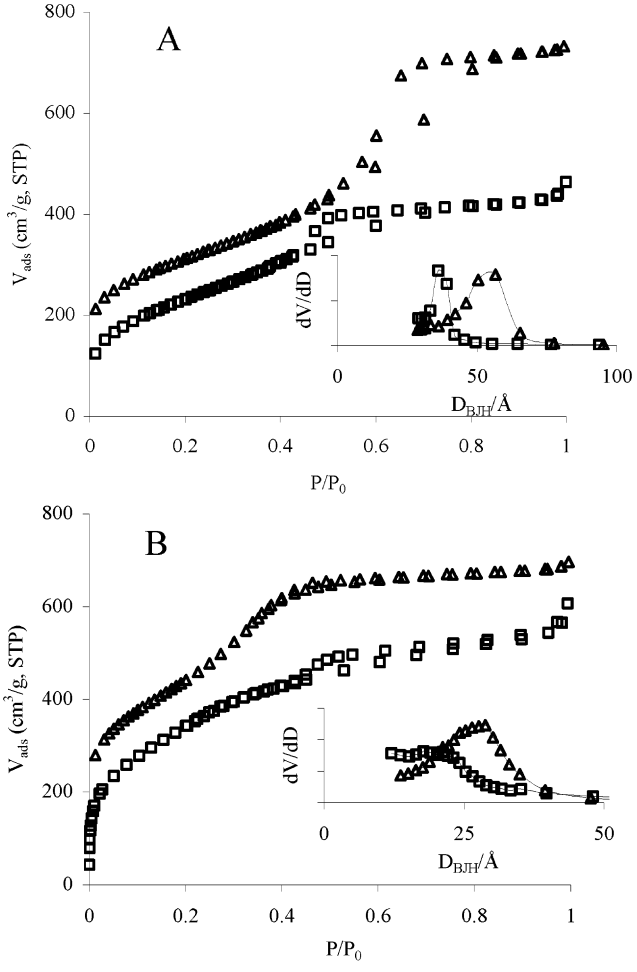

Figure 2. N_2 adsorption−desorption isotherms and corresponding BJH pore size distributions curves (inset) of C_{16}-MS-Br (A) and NNC_{16}-MS-Br (B) prepared at 25 (□) and 70 °C (Δ).

by the corresponding N_2 adsorption−desorption isotherms (Figure 2), which are typical type IV isotherms and clearly display an inflection in the intermediate P/P_0 region, indicating the presence of mesopore channels. Besides, as summarized in Table 1, the very high BET surface areas (in the range of 750−1550 m^2/g), the pore volumes (in the range of 0.5−1.3 cm^3/g), and the narrow mesopore size distributions (Figure 2, inset)

TABLE 1: Textural and Structural Features of C_x-MS-Y and NNC_x-MS-Y as a Function of Chain Length, Type of Acid, and Synthesis Temperature

			BET (m^2/g)		V_{mes} (mL/g)		D (Å)	
	acid	T (°C)	C_{12}	C_{16}	C_{12}	C_{16}	C_{12}	C_{16}
C_x-MS−Y	HCl	25	947	978	0.81	0.70	52.9	50.0
		70	752	854	0.93	0.94	73.1	63.2
	HBr	25	846	858	0.68	0.65	50.0	51.0
		70	794	777	1.26	1.19	87.8	67.9
NNC_x-MS−Y	HCl	25	1205	1234	0.51	0.55	25.0	26.4
		70	1301	1579	0.64	0.74	30.6	29.4
	HBr	25	1299	1286	0.55	0.76	25.0	32.4
		70	1142	1276	0.78	0.87	38.5.	40.1

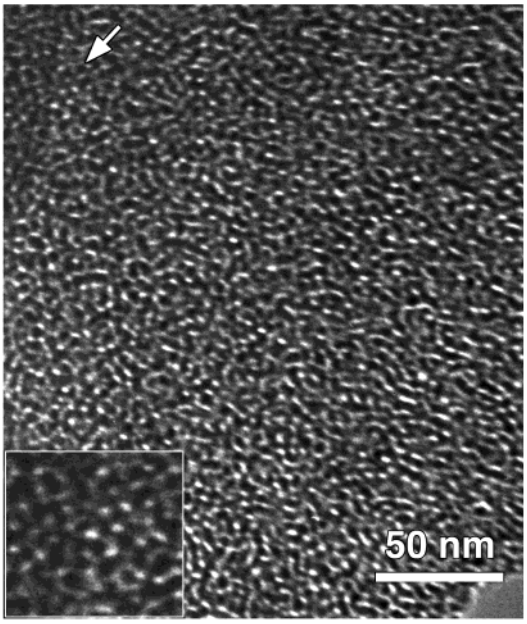

Figure 3. TEM image including inset with higher magnification of calcined NNC_{16}-MS-Br prepared at 70 °C.

with maxima in the range of 20−90 Å are also characteristic of mesoporous materials.

A closer look at Figures 1 and 2 reveals that the XRD patterns and the shape of the N_2 isotherms are very similar to MSU and HMS compounds and are in general indicative of mesostructures possessing nonordered wormlike pore structures with no long-range order symmetry.[10,30,36] Further evidence for the 3D wormhole pore framework is provided by the typical TEM image in Figure 3. This micrograph clearly exhibits disordered wormholelike pores similar to HMS and MSU, and the inset image with higher magnification further shows some local ordering.

In the following sections, the synthesis temperature, type of amine template, and counterion (acid) are changed and the effects of these conditions on the produced mesophases together with the formation mechanism were studied.

(b) Influence of Reaction Temperature. Keeping parameters such as chain length, type of surfactant, and acid constant, it can be seen from Table 1 that the pore diameter and mesopore volume of all synthesized mesoporous materials increase as the synthesis temperature rises from 25 to 70 °C. This is further visualized in Figures 1 and 2, showing the powder X-ray diffraction patterns and the N_2 adsorption−desorption isotherms together with the BJH pore size distributions (inset) of calcined C_{16}-MS-Br and NNC_{16}-MS-Br materials. With increasing assembly temperature, better ordered materials are formed, which is reflected in the increased intensities of the d_{100} reflections

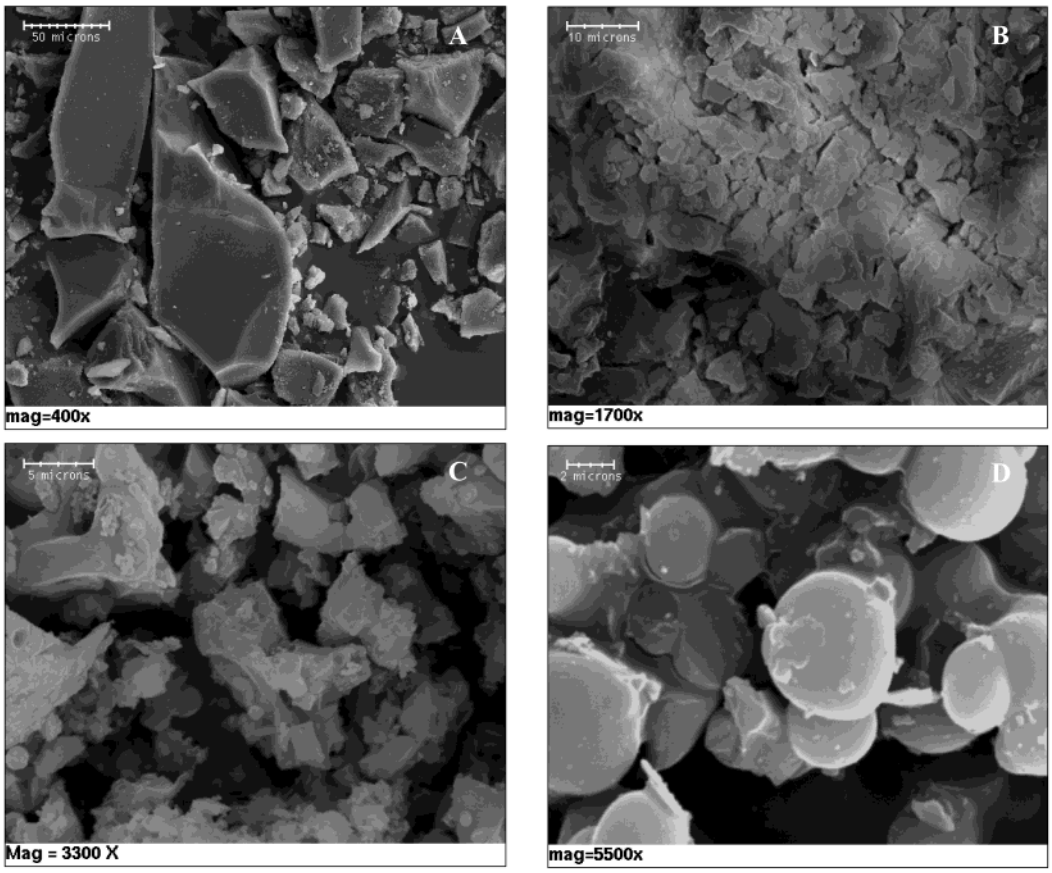

Figure 4. Representative SEM images of NNC_{16}-MS-Br prepared at 25 °C (A) and samples prepared at 70 °C: C_{16}-MS-Br (B), NNC_{16}-MS-Br (C), and NNC_{16}-MS-Cl (D).

shifted to lower 2θ values while the capillary condensation steps get more pronounced and shift to higher P/P_0 values. This observation is in agreement with previously reported research on M41S materials[37] and is consistent with the notion that the hydrophobic cores of the surfactant micelles are increased at higher temperature. SEM images showing the influence of temperature on the NNC_{16}-MS-Br sample are displayed in Figure 4 for materials prepared at 25 (photo A) and 70 °C (photo C). The sample synthesized at ambient temperature consists of large irregular solid blocks in the range of 30−100 μm with both flattened and nicely curved surfaces whereas the sample assembled at 70 °C shows a structure made by agglomeration of fine micrometer-sized solid blocked particles. The formation of relative smaller crystals at higher assembly temperature can be explained by the higher crystallization rate of TEOS.

(c) Influence of Template. Although *N*,*N*-dimethylalkylamines and alkylamines are very similar surfactants, one could expect that, under similar synthesis conditions, mesostructures prepared with *N*,*N*-dimethylalkylamines have larger pores than materials assembled with alkylamines because of the larger surfactant headgroup. However, considering the values of the calculated pore diameters in Table 1, one can observe the opposite trend. For example, the C_{16}-MS-Br sample prepared at 70 °C has a pore diameter of 67.9 Å while the NNC_{16}-MS-Br material has a diameter of merely 40.1 Å. A possible explanation can be found in the hydrophobicity of the headgroups of the surfactants. The *N*,*N*-dimethylalkylamines have a much more hydrophobic headgroup compared to the primary amines because of the two methyl groups bond on the nitrogen atom. Therefore, the relative hydrophilic headgroups of primary alkylamine micelles can easily build up a hydration sphere in aqueous conditions, making these headgroups expand. Figure 4 shows representative SEM micrographs of the C_{16}-MS-Br sample (photo B) and the NNC_{16}-MS-Br sample (photo C) prepared at 70 °C. Both samples consist of irregular particles with magnitudes in the same range (1−10 μm), but the morphology is different. The C_{16}-MS-Br synthesis gives rise to flat "plate"-shaped moieties whereas the NNC_{16}-MS-Br sample consists of agglomerates built up of solid blocks.

(d) Influence of Acid and Formation Mechanism. To gain insight into the influence of the acid (counterion) on the quality of the resulting porous networks, Figure 5 displays the isotherms and BJH pore size distributions of materials synthesized at 70 °C with HCl and HBr for both types of surfactants. For both templates, it can be seen that the influence of the counterion on the shape of the isotherms and the broadness of the pore size distributions is relative small. However, a more detailed examination of the physical data (Table 1) reveals that, for both surfactants, a remarkable decrease in pore diameter and pore volume can be observed for the Cl^--mediated syntheses while the mesoporous framework is better formed when Br^- is used. These observations already imply that, similar to the $S^+X^-I^+$ assembly, the counterion plays an important part in the formation mechanism. Mou et al.[38] investigated the counterion effect in acidic conditions on the formation of mesoporous silica with quaternary ammonium surfactants (S^+). In acid synthesis, the cationic silica precursor (I^+) combines with S^+X^--type active sites whereas the stronger the ion X^- is bonded to S^+, the more it catalyzes the silica condensation into $S^+X^-I^+$. Br^- is in general a much stronger binding anion so a better silica condensation promoter, resulting in the formation of a higher quality mesophase. Based on our observations, a (S^0H^+)(X^-I^+) mechanism can be suggested in which protonated water molecules are hydrogen bonded to the lone electron pairs on

TABLE 2: Effect of Thermal and Hydrothermal Treatment on the Physical Properties of HMS, NNC_{16}-MS-Br and C_{12}-MS-Br

	HMS			NNC_{16}-MS-Br			C_{12}-MS-Br		
treatment conditions	BET (m^2/g)	V_{mes} (mL/g)	D (Å)	BET (m^2/g)	V_{mes} (mL/g)	D (Å)	BET (m^2/g)	V_{mes} (mL/g)	D (Å)
550 °C	1021	0.81	40.0	1276	0.87	40.1	794	1.26	87.8
650 °C	957	0.58	34.8	1131	0.84	39.0	708	1.22	86.2
750 °C	213	*a*	*a*	939	0.68	38.7	704	1.09	85.1
850 °C	*b*	*b*	*b*	772	0.46	35.7	604	0.85	76.0
400 °C, 30 vol % steam, 48 h	915	0.57	35.4	1111	0.75	37.8	727	1.10	81.5
400 °C, 30 vol % steam, 120 h	830	0.48	34.2	1099	0.70	36.7	682	1.04	81.5

[a] No capillary condensation step was observed in the N_2 isotherm. [b] Not measured.

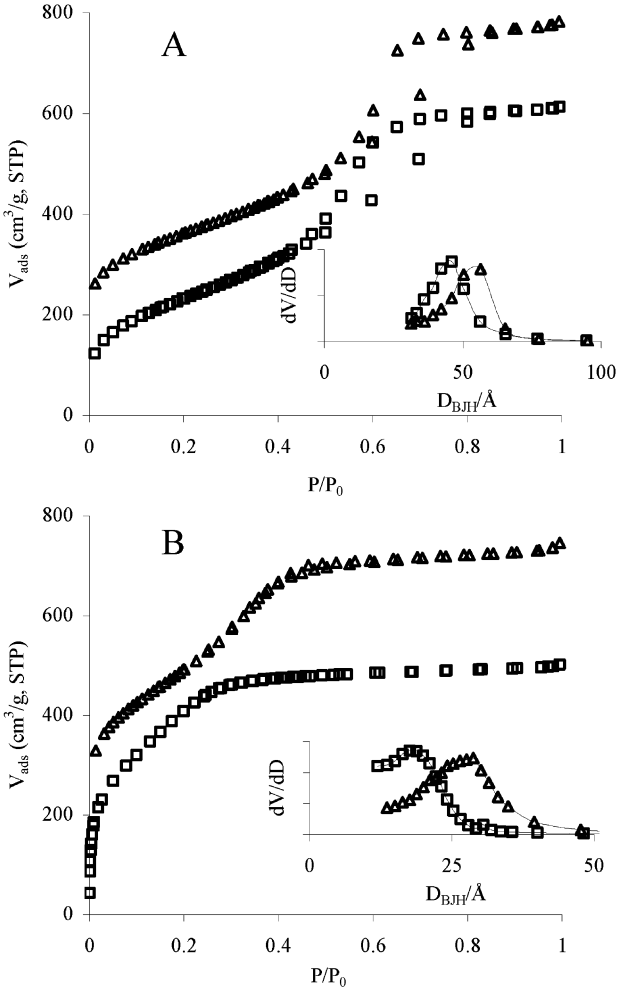

Figure 5. N_2 adsorption−desorption isotherms and corresponding BJH pore size distributions curves (inset) of C_{16}-MS-Y (A) and NNC_{16}-MS−Y (B) prepared at 70 °C with HCl (□) and HBr (Δ) as acids.

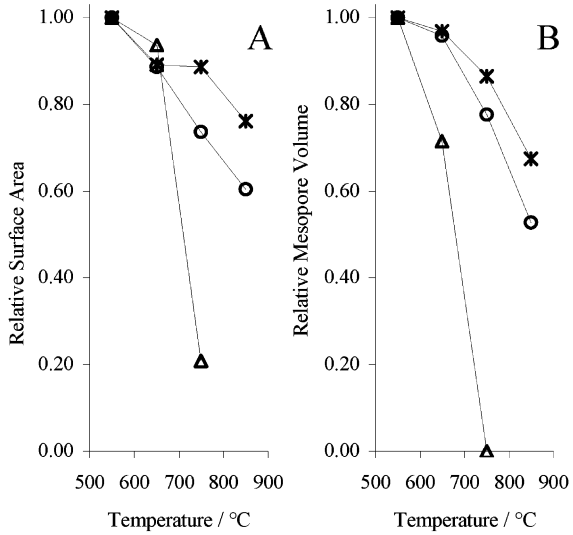

Figure 6. Relative surface area (A) and mesopore volume (B) as a function of temperature for the mesostructures HMS (Δ), C_{12}-MS-Br (*) and NNC_{16}-MS-Br (○).

the amine surfactant headgroups (S^0H^+), which then, similar to S^+, play the role of a cationic surfactant. The counteranion plays a structure-directing role and catalyzes the silica condensation.

Next to the influence of the counterion on the physical properties of the mesostructure, SEM observations also reveal clear differences in particle morphology. SEM images showing the particle texture are displayed in Figure 4 for NNC_{16}-MS-Br (photo C) and NNC_{16}-MS-Cl (photo D), both prepared at 70 °C. The use of Cl^- as counterion leads to nonuniform spherical particles and agglomerates of spherical particles both in the micrometer range whereas Br^- forms agglomerates of solid blocks. This feature can be linked to the formation mechanism including the role of the counterion. Ozin and co-workers[39,40] studied the influence of the reaction conditions on particle shape for materials prepared in acidic conditions and assembled by the $S^+X^-I^+$ mechanism. The formation of a spherical morphology or more irregular forms depends on the balance between the rate of polymerization of inorganic species and the rate of mesostructure formation. In the case of a relative fast polymerization, the morphology is controlled by the deposition of silicate micellar species on specific regions of liquid crystal seeds, resulting in the formation of gyroids or nonuniform agglomerated blocks. By contrast, a slower polymerizing growing silicate liquid crystal seed is driven by global surface tension forces to minimize its surface free energy by forming the shape of a sphere. As mentioned above, Br^- is shown to be a strong binding anion and therefore a fast silica polymerization promoter compared to Cl^-. For the Br^- syntheses, particle growth is therefore controlled by the polymerization rate eventuating in agglomerated solid blocks whereas for Cl^- the particle shape is directed by surface tension forces resulting in more spherical particles.

(e) Thermal and Hydrothermal Stability. To assess thermal and hydrothermal stability, samples synthesized with primary amine (C_{12}-MS-Br) and *N*,*N*-dimethylamine (NNC_{16}-MS-Br), both prepared at 70 °C, are exposed to temperatures up to 850 °C and a flow of steam at 400 °C. To have an indication of the relative stability, both (S^0H^+)(X^-I^+) assembled samples are compared with HMS, which is also prepared with amines as template and TEOS as silica source but formed through the S^0I^0 mechanism. Table 2 presents the physical properties of thermally and hydrothermally treated samples. Figure 6A and B present the relative decrease in BET surface area and mesopore volume, respectively, Figure 7A and B show the N_2 isotherms of HMS and NNC_{16}-MS-Br, respectively, as a function of calcination temperature. At 750 °C, it can be seen from Figure 6 that HMS

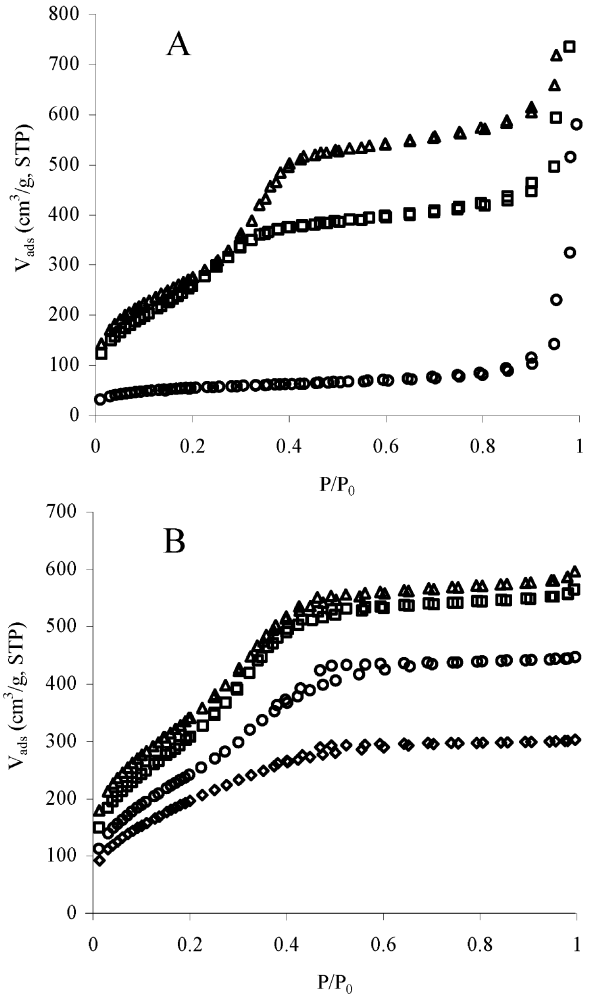

Figure 7. N_2 adsorption−desorption isotherms of HMS (A) and NNC_{16}-MS-Br (B) calcined at 550 (Δ), 650 (□), 750 (○), and 850 °C (◇).

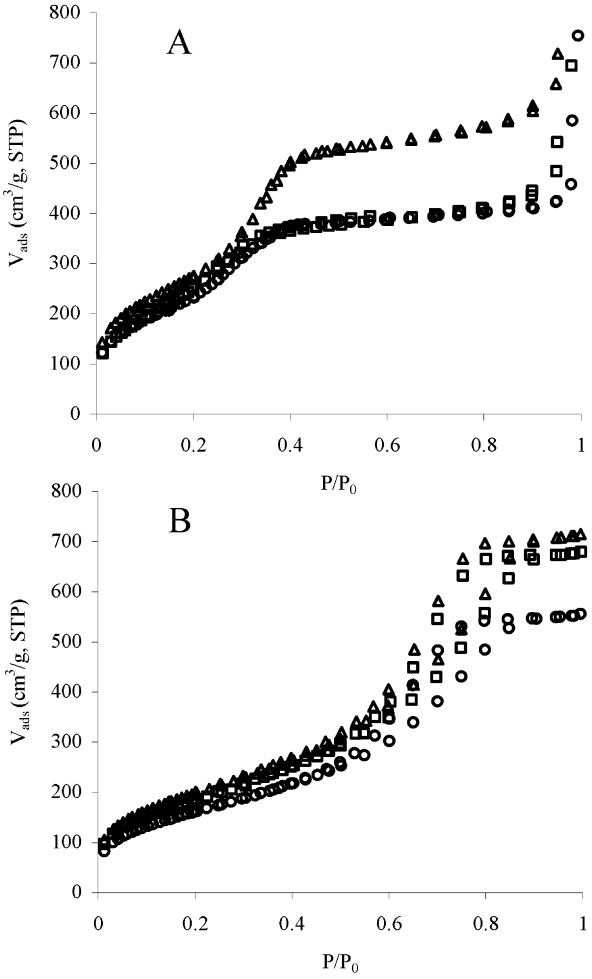

Figure 8. N_2 adsorption−desorption isotherms of HMS (A) and C_{12}-MS-Br (B) hydrothermally treated for 0 (Δ), 48 (□), and 120 h (○).

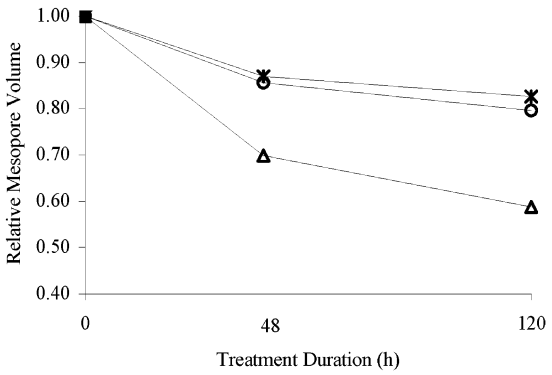

Figure 9. Relative mesopore volume as a function of hydrothermal treatment time for HMS (Δ), C_{12}-MS-Br (*), and NNC_{16}-MS-Br (○).

suffers a decrease in BET surface area of 80%, and in addition, no mesopores can be detected at this point. In constrast, around 70% of the BET surface area and 60% of the pore volume still remain for both (S^0H^+)(X^-I^+) assembled samples after calcination at 850 °C. These differences can also be seen in Figure 7, where the pore structure of HMS is already completely degraded at 750 °C, as reflected in the disappearance of the capillary condensation step and the d_{100} diffraction line (not shown). Despite the decrease in BET surface area and pore volume, the observed textural properties of the isotherms of both (S^0H^+)(X^-I^+) assembled samples remains almost unaffected after subjection to a temperature of 850 °C. In both cases, clear d_{100} diffraction lines can still be observed at 850 °C yet the d_{100} value and the pore diameter are gradually shifted to lower values when the calcination temperature is increased.

When S^0I^0 and (S^0H^+)(X^-I^+) assembled samples are subjected to steam for 48 and 120 h, the N_2 isotherms (Figure 8) and physical characteristics show that a visual degradation of pore diameter, mesopore volume, and BET value has occurred. However, it is interesting to observe that after this treatment the texture of the isotherms remains almost unchanged while in all cases the BET surface areas are merely decreased by about 15−20%. Nevertheless, close inspection of the pore volume data, visualized in Figure 9, clearly indicates significant differences in porosity. The loss in mesoporosity is reflected in a 30% decrease of mesopore volume for HMS after a hydrothermal treatment of 48 h and even a 41% decrease after 120 h, while still ∼80% of the initial mesopore volume remains for both (S^0H^+)(X^-I^+) assembled samples after 120 h. In a previous report,[41] the thermal and hydrothermal stabilities were found to be strongly related to the condensation degree of the silica walls. It is further believed that the structural degradation is caused by the hydrolysis of Si−O−Si bonds[42] where the hydrolysis process for highly polymerized walls is much slower than for low condensed mesostructures. The much higher thermal and hydrothermal stability of (S^0H^+)(X^-I^+) assembled mesostructures compared to HMS can therefore be explained by the differences in synthesis conditions. In the (S^0H^+)(X^-I^+) mechanism, a high condensation of silanol groups to highly

polymerized Si−O−Si bonds is catalyzed by the counterion whereas in the S^0I^0 mechanism no such condensation promoter is available in the reaction medium. Therefore, the $(S^0H^+)(X^-I^+)$ assembled silica mesostructures consist of better-polymerized walls resulting in a higher thermal and hydrothermal stability.

Conclusions

A new pathway toward mesostructured silica has been developed. These materials are assembled from inexpensive and nontoxic nonionic alkylamines and *N*,*N*-dimethylamines in acidic conditions, which afford frameworks with wormlike pore structure with high surface area and large pore volumes. An increase in assembly temperature from 25 to 70 °C gives rise to higher quality materials while the pore diameters for the alkylamine-assembled materials are larger than the *N*,*N*-dimethylalkylamine-prepared structures due to a larger hydration sphere.

It has been shown that the acid plays an important part in the formation mechanism and the morphology. Protonated water molecules are hydrogen bonded to the lone electron pair of the amine surfactant headgroups (S^0H^+) while the counterion X^-, which is bonded to the (S^0H^+), catalyzes the silica polymerization to $(S^0H^+)(X^-I^+)$. Br^- has shown to be a strong binding anion and therefore a fast silica polymerization promoter compared to Cl^-, resulting in a material with better physical properties. We have further shown that, depending on the rate of polymerization of the silica species, the morphology of the mesostructure can be controlled. In the case of Br^-, a fast polymerization promoter, the morphology is controlled by the deposition of silicate micellar species on specific regions of liquid crystal seeds, resulting in the formation of nonuniform agglomerated blocks whereas a slower polymerizing growing silicate liquid crystal seed for the Cl^- syntheses is driven by global surface tension forces to minimize its surface free energy by forming the shape of a sphere. Compared to HMS, which is also prepared with nonionic amines but formed through the S^0I^0 mechanism, these materials exhibit an outstanding thermal and hydrothermal stability because of much better polymerized walls.

Acknowledgment. P.V.D.V. thanks the Fund for Scientific Researsch (FWO, Flanders, Belgium) for a position as senior researcher. T.L. is indebted to the IWT-Flanders-Belgium for a Ph.D. grant.

References and Notes

(1) Kresge, C. T.; Leonowicz, M. E.; Roth, W. J.; Vartuli J. C.; Beck, J. S. *Nature* **1992**, *359*, 710.
(2) Inagaki, S.; Fukushima, Y.; Kuroda, K. *J. Chem. Soc., Chem. Commun.* **1993**, 680.
(3) Ryoo, R.; Kim, J. M.; Ko, C. H.; Shin, C. H. *J. Phys. Chem. B* **1996**, *100*, 17718.
(4) Galarneau, A.; Barodawalla, A.; Pinnavaia, T. J. *Nature* **1995**, *374*, 529.
(5) Tanev, P. T.; Pinnavaia, T. J. *Science* **1995**, *267*, 865.
(6) Tanev, P. T.; Chibwe, M.; Pinnavaia, T. J. *Nature* **1994**, *368*, 321.
(7) Huo, G.; Margolese, D. I.; Ciesla, U.; Feng, P.; Gier, T. E.; Sieger, P.; Leon, R.; Petroff, P. M.; Schüth F.; Stucky, G. D. *Nature* **1994**, *368*, 317.
(8) Zhao, D.; Feng, J.; Huo, Q.; Melosh, N.; Frederickson, G. H.; Chmelka, B. F.; Stucky, G. D. *Science* **1998**, *279*, 548.
(9) Zhao, D.; Huo, Q.; Feng, J.; Chmelka, B. F.; Stucky, G. D., *J. Am. Chem. Soc.* **1998**, *120*, 6024.
(10) Bagshaw, S. A.; Prouzet, E.; Pinnavaia, T. J. *Science* **1995**, *269*, 1242.
(11) Zhang, W.; Pauly, T. R.; Pinnavaia, T. J. *Chem. Mater.* **1997**, *9*, 2491.
(12) Tanev, P. T.; Pinnavaia, T. J. *Science* **1996**, *271*, 1267.
(13) Kim, S. S.; Zhang, W.; Pinnavaia, T. J. *Science* **1998**, *282*, 1302.
(14) Schmidt-Winkel, P.; Lukens, W. W., Jr.; Zhao, D.; Yang, P.; Chmelka, B. F.; Stucky, G. D. *J. Am. Chem. Soc.* **1999**, *121*, 254.
(15) Van Der Voort, P.; Ravikovitch, P. I.; De Jong, K. P.; Neimark, A. V.; Janssen, A. H.; Benjelloun, M.; Van Bavel, E.; Cool, P.; Weckhuysen, B. M.; Vansant, E. F. *Chem. Commun*. **2002**, 1010.
(16) Baltes, M.; Cassiers, K.; Van Der Voort, P.; Weckhuysen, B. M.; Schoonheydt, R. A.; Vansant, E. F. *J. Catal.* **2001**, *197*, 160.
(17) Raimondo, M.; Perez, G.; Sinibaldi, M.; De Stefanis A.; Tomlinson, A. A. G. *J. Chem. Soc., Chem. Commun.* **1997**, *15*, 1343.
(18) Grün, M.; Kurganoz, A. A.; Schacht, S.; Schütz, F.; Unger, K. K. *J. Chromatogr., A* **1996**, *740*, 1.
(19) Huang, M. H.; Choudrey, A.; Yang, P. D. *Chem. Commun*. **2000**, 1063.
(20) Han, Y. J.; Kim, J. M.; Stucky, G. D. *Chem. Mater.* **2000**, *12*, 2068.
(21) Joo, S. H.; Choi, S. J.; Oh, I.; Kwak, J.; Liu, Z.; Terasaki, O.; Ryoo, R. *Nature* **2001**, *412*, 169.
(22) Ryoo,-R.; Joo S. H.; Kruk, M.; Jaroniec, M. *Adv. Mater.* **2001**, *13*, 677.
(23) Lee, J. S.; Joo S. H.; Ryoo, R. *J. Am. Chem. Soc.* **2002**, *124*, 1156.
(24) Stevens, R. M. D.; Frederick, N. A.; Smith, B. L.; Morse, D. E.; Stucky G. D.; Hansma, P. K. *Nanotechnology* **2000**, *11*, 1.
(25) Kleitz, F.; Marlow, F.; Stucky G. D.; Schuth, F. *Chem. Mater.* **2001**, *13*, 3587.
(26) Scott, B. J.; Wirnsberger, G.; McGehee, M. D.; Chmelka, B. F.; Stucky G. D. *Adv. Mater.* **2001,** *13*, 1231.
(27) Cassiers, K.; Van Der Voort, P.; Vansant, E. F. *Chem. Commun*. **2000,** 2489.
(28) Sayari, A. *Chem. Mater.* **1996**, *8*, 1840.
(29) Mokaya, R.; Jones, W. *J. Catal.* **1997**, *172*, 211.
(30) Tanev, P. T.; Pinnavaia T. J., *Chem. Mater.* **1996**, *8*, 2068.
(31) Sing, K. S. W.; Everett, D. H.; Haul, R. A. W.; Moscou, L.; Pierotti, R. A.; Rouquerol, J.; Siemieniewska, T. *Pure Appl Chem.* **1985**, *57*, 603.
(32) Galarneau A.; Desplantier, D.; Dutartre, R.; Di Renzo, F. *Microporous Mesoporous Mater*. **1999**, *27*, 297.
(33) Zhu, H. Y.; Zhao, X. S.; Lu, G. Q.; Do, D. D. *Langmuir* **1996**, *12*, 6513.
(34) Ravikovitch, P. I.; Haller, G. L.; Neimark, A. V. *Adv. Colloid Interface Sci*. **1998**, *77*, 203.
(35) Neimark, A. V.; Ravikovitch, P. I. **2001**, *44*−*45*, 66.
(36) Kim, S.-S.; Pauly, T. R.; Pinnavaia, T. J. *Chem. Commun.* **2000**, 835.
(37) Collart, O.; Van Der Voort, P.; Vansant, E. F.; Desplantier, D.; Galarneau, A.; Di Renzo, F.; Fajula, F. *J. Phys. Chem. B* **2001**, *105*, 12771.
(38) Lin, H.-P.; Kao, C.-P.; Mou, C.-Y. *Microporous Mesoporous Mater*. **2001**, *48*, 135.
(39) Ozin, G. A.; Yang, H.; Sokolov, I.; Coombs, N. *Nature* **1997**, *386*, 692.
(40) Yang, H.; Vovk, G.; Coombs, N.; Sokolov, I.; Ozin, G. A. *J. Mater. Chem.* **1998**, *8*, 743.
(41) Cassiers, K.; Linssen, T.; Mathieu, M.; Benjelloun, M.; Schrijnemakers, K.; Van Der Voort, P.; Cool, P.; Vansant, E. F. *Chem. Mater*. **2002**, *14*, 2317.
(42) Tatsumi, T.; Koyano, K. A.; Tanaka, Y.; Nakata, S. *Chem. Lett.* **1997**, *5*, 469.